Theoretical study on production cross sections of exotic actinide nuclei in multinucleon transfer reactions*

Long Zhu(祝龙)

Sino-French Institute of Nuclear Engineering and Technology, Sun Yat-sen University, Zhuhai 519082, China

Abstract: Within the dinuclear system (DNS) model, the multinucleon transfer reactions ^{129,136}Xe + ^{248}Cm, ^{112}Sn + ^{238}U, and ^{144}Xe + ^{248}Cm are investigated. The production cross sections of primary fragments are calculated with the DNS model. By using a statistical model, we investigate the influence of charged particle evaporation channels on production cross sections of exotic nuclei. It is found that for excited neutron-deficient nuclei the charged particle evaporation competes with neutron emission and plays an important role in the cooling process. The production cross sections of several exotic actinide nuclei are predicted in the reactions ^{112}Sn + ^{238}U and ^{136,144}Xe + ^{248}Cm. Considering the beam intensities, the collisions of ^{136,144}Xe projectiles with a ^{248}Cm target for producing neutron-rich nuclei with Z=92−96 are investigated.

Keywords: transfer reactions, exotic actinide nuclei, charged particle evaporation, dinuclear system model

PACS: 25.40.Hs, 25.70.-z **DOI:** 10.1088/1674-1137/41/12/124102

1 Introduction

Most transuranium isotopes have been produced through neutron capture, light charged particle induced reactions, and heavy ion fusion evaporation reactions [1]. Due to the limitations of neutron fluxes in reactors and available projectile and target combinations, the multinucleon transfer process has arisen as one promising way to produce exotic actinide nuclei [2–4]. Many experiments based on multinucleon transfer reactions with actinide targets were performed around thirty years ago to produce actinide nuclei [5–9], and several Fm and Md neutron-rich isotopes were produced at the level of 0.1 μb. No new isotope was observed. Due to low separation and detection efficiency of the available laboratory equipment at the time, few new heavy isotopes were observed based on multinucleon transfer reactions. However, as it is a promising approach, the multinucleon transfer process has been extensively investigated experimentally [10–21] and theoretically [22–43] in recent years. Recently, five new neutron-deficient isotopes ^{216}U, ^{219}Np, ^{223}Am, ^{229}Am, and ^{233}Bk were observed in the transfer reaction ^{48}Ca + ^{248}Cm [44]. With the improvement of laboratory equipment, the prospects are good not only for production of transuranium and superheavy neutron-rich nuclei but also for production of nuclei in the region of astrophysical interest along the closed N=126 neutron shell. The huge advantages of using the multinucleon transfer process for the production of very neutron-rich nuclei with $N = 126$ were noticed in Ref. [21], which showed that the advantages became more and more striking when the atomic number was lower.

In this paper, the transfer reactions ^{129,136}Xe + ^{248}Cm, ^{112}Sn + ^{238}U, and ^{144}Xe + ^{248}Cm are investigated within the framework of the dinuclear system (DNS) model. The influence of charged particle emission on the production of neutron-deficient nuclei is studied. The production of unknown actinide isotopes in the reactions ^{112}Sn + ^{238}U and ^{144}Xe + ^{248}Cm is predicted.

The article is organized as follows. In Section 2, we give a detailed description of the DNS model. The results and discussion are presented in Section 3. Finally, we summarize the main results in Section 4.

2 Description of the model

The DNS model has been successfully used to describe the multinucleon transfer process [23–33] and the synthesis of superheavy nuclei [45–51]. In the DNS model, the distribution probability $P(Z_1,N_1,t)$ for fragment 1 with proton number Z_1 and neutron number N_1 at time t can be calculated by solving the master equation in the potential energy surface (PES). The master equation can be written as

$$\frac{\mathrm{d}P(Z_1,N_1,t)}{\mathrm{d}t} = \sum_{Z_1'} W_{Z_1,N_1;Z_1',N_1}(t)[d_{Z_1,N_1}P(Z_1',N_1,t) - d_{Z_1',N_1}P(Z_1,N_1,t)]$$

Received 18 August 2017

∗ Supported by National Natural Science Foundation of China (11605296) and Natural Science Foundation of Guangdong Province, China (2016A030310208)

$$+\sum_{N_1'} W_{Z_1,N_1;Z_1,N_1'}(t)[d_{Z_1,N_1}P(Z_1,N_1',t) - d_{Z_1,N_1'}P(Z_1,N_1,t)]. \quad (1)$$

Here $W_{Z_1,N_1;Z_1',N_1}$ ($W_{Z_1,N_1;Z_1,N_1'}$) denotes the mean transition probability from the channel (Z_1, N_1) to (Z_1', N_1) [or (Z_1, N_1) to (Z_1, N_1')], and d_{Z_1,N_1} is the microscopic dimension (the number of channels) corresponding to the macroscopic state (Z_1, N_1) [52]. The sum is taken over all possible proton and neutron numbers that fragment 1 may take, but only one nucleon is considered in the model ($Z_1'=Z_1\pm1$; $N_1'=N_1\pm1$). The transition probability is related to the local excitation energy, and can be written as

$$W_{Z_1,N_1;Z_1',N_1}(t)= \frac{\tau_{\rm mem}(Z_1,N_1,E^*_{\rm DNS}(Z_1,N_1);Z_1',N_1,E^*_{\rm DNS}(Z_1',N_1))}{d_{Z_1,N_1}d_{Z_1',N_1}\hbar^2}\times \sum_{ii'}|\langle Z_1',N_1,E^*_{\rm DNS}(Z_1',N_1),i'|V(t)|Z_1,N_1,E^*_{\rm DNS}(Z_1,N_1),i\rangle|^2. \quad (2)$$

Here, $E^*_{\rm DNS}$ is the local excitation energy. i denotes the remaining quantum numbers. The detailed descriptions of $\tau_{\rm mem}$ and $V(t)$ can be seen in Ref. [53]. The transition probability expression is similar to that for neutron transitions.

The local excitation energy of the DNS can be written as

$$E^*_{\rm DNS}(Z_1,N_1)=E_{\rm diss}-[U(Z_1,N_1,R_{\rm cont})-U(Z_{\rm p},N_{\rm p},R_{\rm cont})], \quad (3)$$

where $E_{\rm diss}$ is the energy dissipated into the composite system from the incident energy, which depends on entrance angular momentum J and incident energy. $E_{\rm diss}$ strongly influences the fragment distribution. For large values of $E_{\rm diss}$, the barrier can be easily overcome to produce exotic primary fragments. The subscript "p" denotes the initial configuration of the DNS.

The PES can be written as

$$U(Z_1,N_1,R_{\rm cont})=B(Z_1,N_1)+B(Z_2,N_2) +V_{\rm cont}(Z_1,N_1,R_{\rm cont}), \quad (4)$$

where $B(Z_i,N_i)$ ($i=1$, 2) is the ground state binding energy of the fragment i. The effective nucleus-nucleus interaction potential $V_{\rm cont}(Z_1,N_1,R_{\rm cont})$ can be written as

$$V_{\rm cont}(Z_1,N_1,R_{\rm cont})=V_{\rm N}(Z_1,N_1,R_{\rm cont}) +V_{\rm C}(Z_1,N_1,R_{\rm cont}). \quad (5)$$

For reactions with no potential pockets, the position where the nucleon transfer process takes place can be found with the equation: $R_{\rm cont}=R_1(1+\beta_1Y_{20}(\theta_1))+R_2(1+\beta_2Y_{20}(\theta_2))+0.7$ fm. Here, $R_{1,2}=1.16A_{1,2}^{1/3}$. $\beta_{1,2}$ is the quadrupole deformation parameter of the fragments and is taken from Ref. [54]. As an example, Figure 1 shows the driving potentials for the reaction ^{129}Xe + ^{248}Cm in tip-tip and side-side orientations. The arrow shows the position of the entrance channel. One valley corresponding to the doubly magic fragment ^{208}Pb can be clearly seen in the side-side orientation. In this work, we investigate the dissipation process under the PES with tip-tip orientation. For tip-tip collisions, we take $\theta_i=0$.

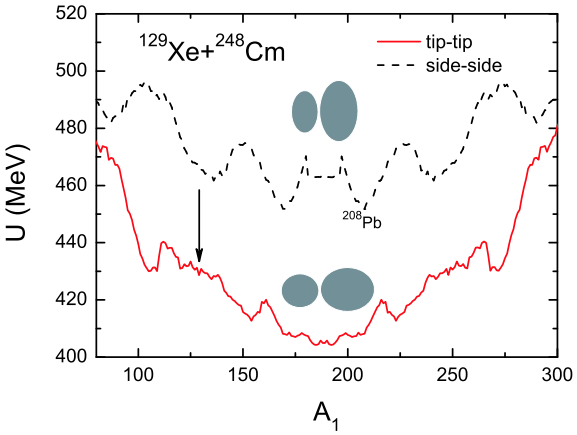

Fig. 1. (color online) The PES for the reaction ^{129}Xe + ^{248}Cm in tip-tip (solid) and side-side (dashed) orientations. The arrow indicates the entrance channel.

The nuclear potential can be written as [55, 56]

$$V_{\rm N}(r,\theta)=C_0\left\{\frac{F_{\rm in}-F_{\rm ex}}{\rho_0}\left[\int\rho_1^2(\boldsymbol{r})\rho_2(\boldsymbol{r}-\boldsymbol{R})d\boldsymbol{r} +\int\rho_1(\boldsymbol{r})\rho_2^2(\boldsymbol{r}-\boldsymbol{R})d\boldsymbol{r}\right]+F_{\rm ex}\int\rho_1(\boldsymbol{r})\rho_2(\boldsymbol{r}-\boldsymbol{R})d\boldsymbol{r}\right\}, \quad (6)$$

with

$$F_{\rm in,ex}=f_{\rm in,ex}+f'_{\rm in,ex}\frac{N_1-Z_1}{A_1}\frac{N_2-Z_2}{A_2}. \quad (7)$$

Here, $C_0=300$ MeV, $f_{\rm in}=0.09$, $f_{\rm ex}=-2.59$, $f'_{\rm in}=0.42$, and $f'_{\rm ex}=0.54$. Z_1 (N_1) and Z_2 (N_2) are the charge (neutron) number of light and heavy fragments, respectively. The density distributions of two nuclei are expressed as a Woods-Saxon distribution as

$$\rho_1(\boldsymbol{r})=\frac{\rho_0}{1+\exp[(\boldsymbol{r}-\Re_1(\theta_1))/a_1]} \quad (8)$$

and

$$\rho_2(\boldsymbol{r}-\boldsymbol{R})=\frac{\rho_0}{1+\exp[(|\boldsymbol{r}-\boldsymbol{R}|-\Re_2(\theta_2))/a_2]}. \quad (9)$$

Here, $\rho_0=0.16$ fm^{-3}. $\Re_i=R_i[1+\beta_iY_{20}(\theta_i)]$ is the surface radii of the collision nuclei. β_i and R_i are the quadrupole deformation parameter and the spherical radius of the ith nucleus, respectively. The diffuseness parameter is

0.6 fm. $\boldsymbol{R}$ is the distance between the centers of two fragments.

The Coulomb potential is taken as the form in Ref. [57]

$$V_{\rm C}(r,\theta_i)=\frac{Z_1Z_2e^2}{r}+\left(\frac{9}{20\pi}\right)^{1/2}\left(\frac{Z_1Z_2e^2}{r^3}\right)\times\sum_{i=1}^{2}R_i^2\beta_2^{(i)}P_2(\cos\theta_i)+\left(\frac{3}{7\pi}\right)\left(\frac{Z_1Z_2e^2}{r^3}\right)\sum_{i=1}^{2}R_i^2[\beta_2^{(i)}P_2(\cos\theta_i)]^2. \tag{10}$$

The production cross sections of the primary products in transfer reactions can be calculated as follows:

$$\sigma_{\rm pr}(Z_1,N_1)=\frac{\pi\hbar^2}{2\mu E_{\rm c.m.}}\sum_{J=0}^{J_{\max}}(2J+1)T_{\rm cap}\times P(Z_1,N_1,t=\tau_{\rm int}), \tag{11}$$

where $T_{\rm cap}$ is the capture probability. Because there are no potential pockets for multinucleon transfer reactions in this work and the incident energies are above the interaction potentials at the contact configurations (there are no ordinary barriers: the potential energies of these nuclei are repulsive everywhere), it is reasonable to take the value of $T_{\rm cap}$ as 1. The interaction time $\tau_{\rm int}$, which is determined by the deflection function method [58], is strongly affected by interaction potential at the contact configuration, incident energy, and entrance angular momentum J. To calculate the cross sections of secondary products, the deexcitation of primary fragments produced at each angular momentum is considered.

The survival probability of the excited fragments in the process of cooling by means of evaporation of x particles in a certain sequence s, in competition with fission, is estimated usually within the statistical model of atomic nuclei and can be written as [59]

$$W_{\rm sur}^{s}(E^*)=P^{s}(E^*)\times\prod_{i_{\rm s}=1}^{x}\left[\frac{\Gamma_{i_{\rm s}}(E_{i_{\rm s}}^*)}{\Gamma_{\rm tot}(E_{i_{\rm s}}^*)}\right], \tag{12}$$

where E^* is the excitation energy of one primary fragment. Assuming thermal equilibrium, the sharing of the excitation energy between primary fragments is assumed to be proportional to their masses. $i_{\rm s}$ is the index of the evaporation step. $E_{i_{\rm s}}^*$ is the excitation energy before evaporation of the $i_{\rm s}$th step, which can be calculated from the equation $E_{i_{\rm s}+1}^*=E_{i_{\rm s}}^*-B_{i_{\rm s}}-2T_{i_{\rm s}}$. $B_{i_{\rm s}}$ is the separation energy of a particle at the $i_{\rm s}$th step. $T_{i_{\rm s}}$ is the nuclear temperature before the $i_{\rm s}$th step evaporation and is obtained from $E_{i_{\rm s}}^*=aT_{i_{\rm s}}^2-T_{i_{\rm s}}$. The probabilities of evaporating more than one charged particle and of the emission of deuterons are very small. Therefore, the evaporation channels with charged particles are $1pxn$ and $1\alpha xn$ with $x=0-10$ in this work. All the possible sequences are taken into account, since the alpha particle or the proton can be emitted at any step of the evaporation sequence. The realization probability $P^s(E^*)$ can be seen in Ref. [60]. $\Gamma_{\rm tot}=\Gamma_{\rm n}+\Gamma_{\rm f}+\Gamma_{\rm p}+\Gamma_{\alpha}$.

The partial decay widths of the compound nucleus for the evaporation of the light particle ν=(n, p, α) can be estimated using the Weisskopf-Ewing theory [61, 62]

$$\Gamma_{\nu}(E_{i_{\rm s}}^*,J)=\frac{2s_{\nu}+1}{2\pi\rho(E_{i_{\rm s}}^*,J)}\frac{2m_{\nu}R^2}{\hbar^2}\times\int_0^{E_{i_{\rm s}}^*-B_{\nu}^{i_{\rm s}}-\delta}\varepsilon_{\nu}T_{\nu}(\varepsilon_{\nu})\rho(E_{i_{\rm s}}^*-B_{\nu}^{i_{\rm s}}-\varepsilon_{\nu},J){\rm d}\varepsilon_{\nu}. \tag{13}$$

Here, s_{ν}, R, and m_{ν} are the spin of the evaporated light particle, radius of the daughter nucleus B, and mass of the light particle, respectively. $T_{\nu}=\{1+\exp[-\frac{2\pi}{\hbar\omega_B}(\varepsilon_{\nu}-V_{\nu})]\}^{-1}$ is the penetration probability of the Coulomb barrier for evaporating charged particles. The Coulomb barrier for charged particle emission is calculated as shown in Ref. [59]. $R_{\nu}=1.16\times(A_B^{1/3}+A_{\nu}^{1/3})$. T_{ν} is unity for evaporation of neutrons.

The fission decay width is usually calculated within the Bohr-Wheeler (BW) transition-state method [63]:

$$\Gamma_{\rm f}(E_{i_{\rm s}}^*,J)=\frac{1}{2\pi\rho(E_{i_{\rm s}}^*,J)}\times\int_0^{E_{i_{\rm s}}^*-B_{\rm f}^{i_{\rm s}}}\frac{\rho(E_{i_{\rm s}}^*-B_{\rm f}^{i_{\rm s}}-\varepsilon_{\rm f}){\rm d}\varepsilon_{\rm f}}{1+\exp[2\pi(\varepsilon_{\rm f}+B_{\rm f}^{i_{\rm s}}-E_{i_{\rm s}}^*)/\hbar\omega]}. \tag{14}$$

In this work, the fission barrier is obtained by $B_{\rm f}(E^*)=B_{\rm f}^{\rm mac}-\Delta E_{\rm shell}{\rm e}^{-E^*/E_{\rm d}}$. $\Delta E_{\rm shell}$ is the shell correction to the nucleus ground state. The macroscopic part of the fission barrier $B_{\rm f}^{\rm mac}$ is calculated using the liquid drop model [64]. The damping parameter $E_{\rm d}=18.5$ MeV.

The level density is calculated with the Fermi-gas model [65] as

$$\rho(E^*,J)=\frac{2J+1}{24\sqrt{2}\sigma^3a^{1/4}(E^*-\delta)^{5/4}}\times\exp\left[2\sqrt{a(E^*-\delta)}-\frac{(J+1/2)^2}{2\sigma^2}\right], \tag{15}$$

where $\sigma^2=6\bar{m}^2\sqrt{a(E^*-\delta)}/\pi^2$ and $\bar{m}\approx0.24A^{2/3}$. The level density parameter $a=A/10$ MeV^{-1}.

3 Results and discussion

Figure 2 shows a comparison of calculated production cross sections and experimental data [9] for actinide nuclei with $Z=93$–99 in the reactions ^{129,136}Xe + ^{248}Cm. The calculated results show very good agreement with the experimental data, for both the magnitude and the peak positions.

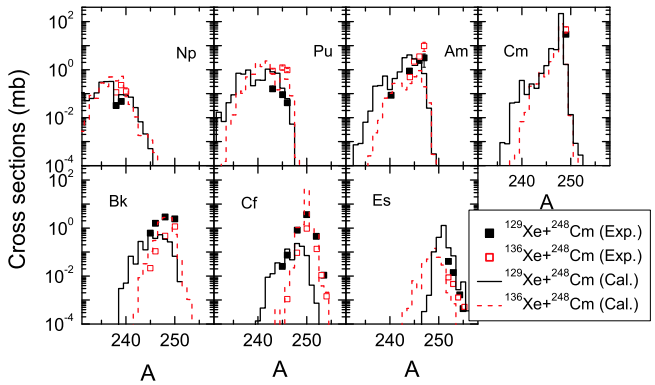

Fig. 2. (color online) Comparison of calculated production cross sections with experimental data [9] for the various target-like fragments (TLFs) in the reactions ^{129,136}Xe + ^{248}Cm. The incident energies ($E_{\rm c.m.}$) for the reactions ^{129}Xe + ^{248}Cm and ^{136}Xe + ^{248}Cm are 513 and 496 MeV, respectively.

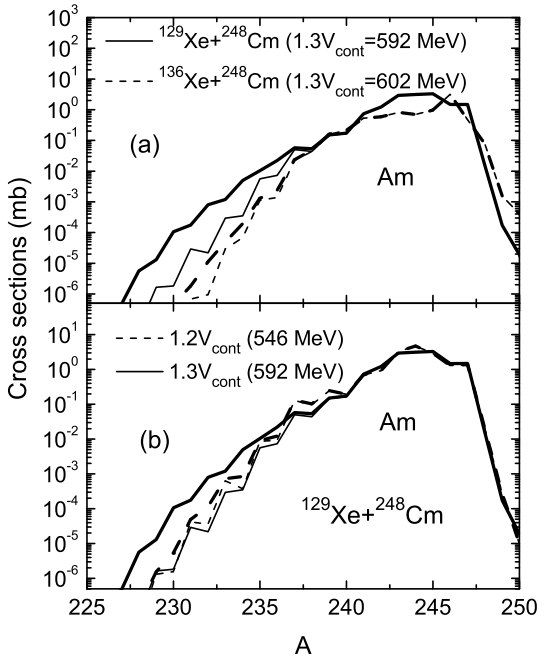

Fig. 3. (a) Calculated cross sections for formation of americium isotopes (Z=95) in ^{129}Xe + ^{248}Cm (solid lines) and ^{136}Xe + ^{248}Cm (dashed lines) collisions. The incident energies for the ^{129}Xe + ^{248}Cm and ^{136}Xe + ^{248}Cm reactions are 592 and 602 MeV, respectively. (b) Calculated cross sections for formation of americium isotopes (Z=95) in ^{129}Xe + ^{248}Cm collisions with different incident energies. In (a) and (b), the thin and thick lines denote the results without and with charged particle evaporation, respectively.

To investigate the influence of charged particle evaporation channels on cross sections in multinucleon transfer reactions, we show in Fig. 3(a) the production cross sections of americium isotopes in ^{129}Xe + ^{248}Cm and ^{136}Xe + ^{248}Cm reactions. The incident energies are chosen as 1.3 times $V_{\rm cont}$, which are 592 and 602 MeV for ^{129}Xe + ^{248}Cm and ^{136}Xe + ^{248}Cm reactions, respectively. The influence of charged particle evaporation can only be seen in the neutron-deficient region and the influence is stronger for more neutron-deficient nuclei. The competition between charged particle evaporation channels and neutron emission for excited neutron-deficient nuclei has been studied in Ref. [59]. Here, we notice that the cross sections are enhanced in the neutron-deficient region for both reactions when consider the charged particle evaporation channels. For neutron-deficient heavy nuclei, the neutron separation energy is positive and much larger than the proton and alpha particle separation energies. For example, the neutron, proton, and alpha particle separation energies of the neutron-deficient nucleus ^{230}Am* are 7.251, 1.909, and -7.651 MeV, respectively. The neutron separation energy is positive and much larger than the others. The alpha particle separation energy is even negative. Therefore, although proton or alpha particle emission from a heavy nucleus is suppressed by the Coulomb barrier, survival probabilities in evaporation channels with proton or alpha particle could be larger than those in pure neutron emission channels for neutron-deficient nuclei with large excitation energies. As shown in Fig. 4, the survival probabilities of ^{230}Am* in evaporation channels with charged particles show great advantages in the cooling process, especially in the high excitation energy region.

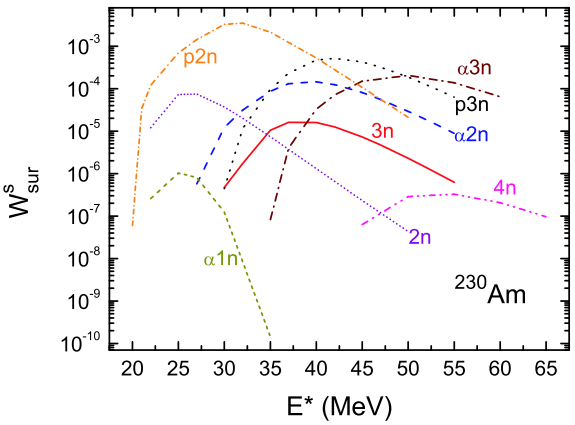

Fig. 4. (color online) The survival probabilities of ^{230}Am* in different evaporation channels with J=0.

In Fig. 3(a), it is found that the influence of charged particle evaporation channels on production cross sections of neutron-deficient nuclei in the reaction ^{129}Xe + ^{248}Cm with lower N/Z value of the projectile is stronger than that in the reaction ^{136}Xe + ^{248}Cm, although the incident energy of ^{129}Xe + ^{248}Cm is a little lower. This is because it is more favorable to produce neutron-deficient

actinide nuclei in the reaction ^{129}Xe + ^{248}Cm, due to the lower N/Z value of the projectile ^{129}Xe. Furthermore, most neutron-deficient actinide nuclei are highly excited due to positive and large Q_{gg} values in the reaction ^{129}Xe + ^{248}Cm. Figure 3(b) shows the production cross sections of americium isotopes in ^{129}Xe + ^{248}Cm reactions with incident energies 546 and 592 MeV. It can be seen that the probability of evaporating charged particles is larger for higher incident energy.

To produce neutron-deficient actinide nuclei, a neutron-deficient projectile would be better. Figure 5 shows the predicted cross sections for producing unknown neutron-deficient nuclei with $Z = 93-97$ in the reaction ^{112}Sn + ^{238}U. The incident energy dependence of cross sections in the neutron-rich region is very weak. The yields of primary fragments are larger for higher incident energy. However, with increasing excitation energies of primary fragments, more neutrons could be evaporated, which can counteract the increased cross sections of primary fragments. The influence of incident energy in the neutron-deficient region is pronounced. We predict that the unknown neutron-deficient nuclei ^{220}Np, ^{221}Np, ^{222}Np, ^{223}Np, and ^{224}Np can be produced in the reaction ^{112}Sn + ^{238}U at $E_{\rm c.m.}$=550 MeV, with cross sections 0.040, 0.041, 1.0, 0.96, and 2.3 μb, respectively. ^{223}Pu, ^{224}Pu, ^{225}Pu, ^{226}Pu, and ^{227}Pu can be produced with cross sections 0.053, 0.073, 0.30, 0.29, and 1.2 μb, respectively. The predicted cross sections of ^{228}Am, ^{229}Am, ^{231}Cm, ^{232}Cm, ^{232}Bk, and ^{233}Bk are 0.079, 0.088, 0.52, 0.90, 0.022, and 0.066 μb, respectively.

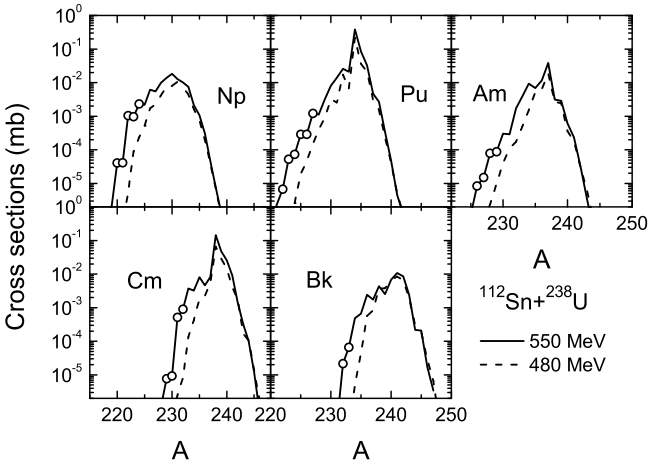

Fig. 5. Predicted cross sections for formation of actinide nuclei with Z=93–97 in the reaction ^{112}Sn + ^{238}U with different incident energies. The circles denote unknown neutron-deficient nuclei under $E_{\rm c.m.}$=550 MeV.

Figure 6 shows cross sections for the production of neutron-rich actinide nuclei in the radioactive beam ^{144}Xe induced reaction ^{144}Xe + ^{248}Cm and the stable beam ^{136}Xe induced reaction ^{136}Xe + ^{248}Cm. The advantages of the cross sections in the reaction ^{144}Xe + ^{248}Cm become more obvious for the production of neutron-rich nuclei with lower charge. For producing neutron-rich americium and curium isotopes, the cross sections of the two reactions are very close. The predicted production cross sections of the unknown neutron-rich nuclei ^{244}U, ^{245}U, ^{246}U, ^{247}U, and ^{248}U in the reaction ^{144}Xe + ^{248}Cm (^{136}Xe + ^{248}Cm) are 3423 μb (0.35 μb), 43.7 μb (0.046 μb), 2.1 μb, 0.040 μb, and 0.013 μb, respectively. ^{245}Np, ^{246}Np, ^{247}Np, ^{248}Np, and ^{249}Np can be produced in the reaction ^{144}Xe + ^{248}Cm (^{136}Xe + ^{248}Cm) with cross sections 3654 μb (1.04 μb), 26.7 μb (0.17 μb), 1.9 μb, 0.11 μb, and 0.036 μb, respectively. ^{248}Pu, ^{249}Pu, ^{250}Pu, and ^{251}Pu can be produced in the reaction ^{144}Xe + ^{248}Cm (^{136}Xe + ^{248}Cm) with cross sections 10.3 μb (0.15 μb), 0.58 μb (0.046 μb), 0.13 μb, and 0.014 μb, respectively. ^{249}Am, ^{250}Am, ^{251}Am, ^{252}Am, and ^{253}Cm can be produced in the reaction ^{144}Xe + ^{248}Cm (^{136}Xe + ^{248}Cm) with cross sections 7.3 μb (0.34 μb), 0.27 μb (0.19 μb), 0.073 μb (0.14 μb), 0.018 μb (0.024 μb), and 0.045 μb (0.13 μb), respectively.

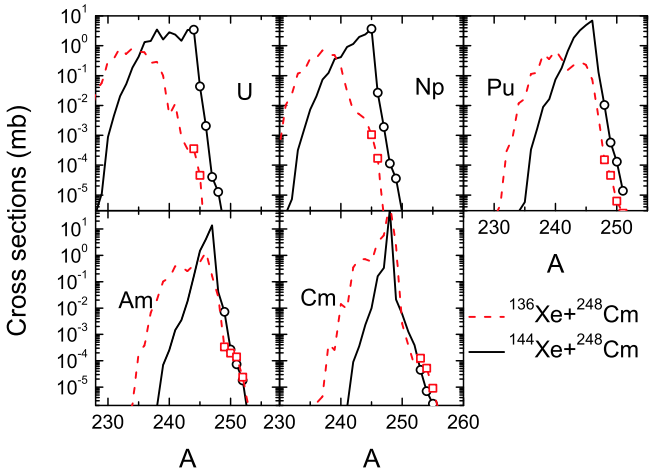

Fig. 6. (color online) Predicted cross sections for formation of actinide nuclei with $Z = 92-96$ in the reactions ^{136}Xe + ^{248}Cm and ^{144}Xe + ^{248}Cm. The incident energies for the reactions ^{136}Xe + ^{248}Cm and ^{144}Xe + ^{248}Cm are 510 and 500 MeV, respectively. The circles and squares denote unknown neutron-rich nuclei.

We show the values of "cross section×beam intensity" for the production of several unknown neutron-rich nuclei with $Z = 92-96$ in the reactions ^{136}Xe + ^{248}Cm and ^{144}Xe + ^{248}Cm in Fig. 7. The beam intensities are obtained from Ref. [66]. It can be seen that the collisions of target ^{248}Cm with stable beam ^{136}Xe show great advantages for producing unknown neutron-rich nuclei with $Z = 93-96$, in comparison with the radioactive beam ^{144}Xe induced reaction. Although the production cross sections are enhanced in the radioactive beam ^{144}Xe

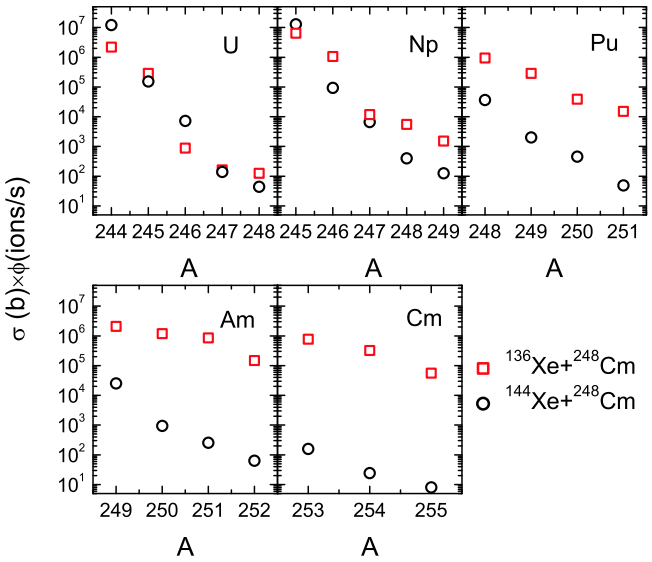

Fig. 7. (color online) "Cross section×beam intensity" ($\sigma\times\phi$) factor in ^{136}Xe + ^{248}Cm and ^{144}Xe + ^{248}Cm reactions for production of unknown nuclei as shown in Fig 6.

induced reaction as shown in Fig. 6, due to very low beam intensity the values of $\sigma\times\phi$ factor are lower than those in the stable beam ^{136}Xe induced reaction. However, with decreasing charge number of the objective nucleus (increasing number of protons picked up from target to projectile), the discrepancy of the $\sigma\times\phi$ value between the ^{136}Xe + ^{248}Cm and ^{144}Xe + ^{248}Cm reactions becomes smaller and smaller. The advantages of a radioactive beam for production of several uranium neutron-rich isotopes can be seen. The same behavior is also shown in Ref. [25]. We can expect that for producing neutron-rich nuclei with $Z<92$, higher production rates can be shown in the reaction ^{144}Xe + ^{248}Cm than those in the reaction ^{136}Xe + ^{248}Cm. This is mainly due to the more obvious advantages of production cross sections for producing nuclei with lower charge number in the ^{144}Xe induced reaction, as shown in Fig. 6.

4 Conclusions

The production cross sections of neutron-deficient and neutron-rich actinide nuclei in multinucleon transfer reactions have been investigated within the framework of the DNS model. The influence of charged particle evaporation channels on production cross sections have been studied in ^{129,136}Xe + ^{248}Cm reactions. For the more neutron-deficient system, ^{129}Xe + ^{248}Cm, the influence of charged particle channels on production cross sections of neutron-deficient actinide nuclei is stronger. For producing neutron-deficient actinide nuclei, charged particle evaporation channels play an important role in the process of deexcitation. In the neutron deficient region, the charged particle evaporation channels compete with neutron emission, and the probability of evaporating charged particles increases with increasing incident energy. The unknown neutron-deficient actinide nuclei produced in the reaction ^{112}Sn + ^{238}U are predicted. We have also predicted the production cross sections of several neutron-rich actinide nuclei in the reaction ^{136,144}Xe + ^{248}Cm. It is found that many unknown nuclei can be produced at the level of μb to mb. The production of neutron-rich nuclei with $Z=92-96$ in collisions of ^{136,144}Xe projectiles with a ^{248}Cm target has been investigated, considering the beam intensities as well. It is found that the stable beam ^{136}Xe induced reaction ^{136}Xe + ^{248}Cm is better for producing neutron-rich nuclei with Z=93–96, in comparison to the reaction ^{144}Xe + ^{248}Cm. However, the radioactive beam ^{144}Xe is expected to be better for producing neutron-rich nuclei with a much lower charge number than the target.

References

1 M. Thoennessen, Rep. Prog. Phys., **76**: 056301 (2013)
2 V. V. Volkov, Phys. Rep., **44**: 93 (1978)
3 H. Freiesleben and J. V. Kratz, Phys. Rep., **106**: 1 (1984)
4 J. V. Kratz, W. Loveland, and K. J. Moody, Nucl. Phys. A, **944**: 117 (2015)
5 K. D. Hildenbrand, H. Freiesleben, F. Pühlhofer, W. F. W. Schneider, R. Bock, D. v. Harrach, and H. J. Specht, Phys. Rev. Lett., **39**: 1065 (1977)
6 M. Schädel et al, Phys. Rev. Lett., **41**: 469 (1978)
7 M. Schädel et al, Phys. Rev. Lett., **48**: 852 (1982)
8 K. J. Moody et al, Phys. Rev. C, **33**: 1315 (1986)
9 R. B. Welch and K. J. Moody et al, Phys. Rev. C, **35**: 204 (1987)
10 D. C. Rafferty, et al, Phys. Rev. C, **94**: 024607 (2016)
11 W. Loveland, A. M. Vinodkumar, D. Peterson, and J. P. Greene, Phys. Rev. C, **83**: 044610 (2011)
12 J. V. Kratz, M. Schädel, and H. W. Gäggeler, Phys. Rev. C, **88**: 054615 (2013)
13 A. Vogt et al, Phys. Rev. C, **92**: 024619 (2015)
14 L. Chen et al, Phys. Lett. B, **691**: 234 (2010)
15 J. Kurcewicz et al, Phys. Lett. B, **717**: 371 (2012)
16 E. M. Kozulin et al, Phys. Rev. C, **89**: 014614 (2014)
17 M. V. Pajtler et al, Nucl. Phys. A, **941**: 273 (2015)
18 W. Królas et al, Nucl. Phys. A, **832**: 170 (2010)
19 E. M. Kozulin et al, Phys. Rev. C, **86**: 044611 (2012)
20 J. S. Barrett et al, Phys. Rev. C, **91**: 064615 (2015)
21 Y. X. Watanabe et al, Phys. Rev. Lett., **115**: 172503 (2015)
22 V. Zagrebaev and W. Greiner, Phys. Rev. Lett., **101**: 122701 (2008)
23 Z. Q. Feng, G. M. Jin, and J. Q. Li, Phys. Rev. C, **80**: 067601 (2009)
24 Z. Q. Feng, Phys. Rev. C, **95**: 024615 (2017).
25 L. Zhu et al, Phys. Lett. B, **767**: 437 (2017)
26 L. Zhu, et al, Phys. Rev. C, **94**: 054606 (2016)
27 L. Zhu, et al, Phys. Rev. C, **95**: 044608 (2017)
28 L. Zhu, et al, Nucl. Phys. A, **964**: 93 (2017)
29 L. Zhu, et al, Phys. Rev. C, **96**: 024606 (2017)
30 G. G. Adamian, N. V. Antonenko, and D. Lacroix, Phys. Rev.

C, **82**: 064611 (2010)
31 L. Zhu, Z. Q. Feng, and F. S. Zhang, J. Phys. G: Nucl. Part. Phys., **42**: 085102 (2015)
32 G. G. Adamian, N. V. Antonenko, and A. S. Zubov, Phys. Rev. C, **71**: 034603 (2005)
33 Yu. E. Penionzhkevich, G. G. Adamian, and N. V. Antonenko, Phys. Lett. B, **621**: 119 (2005)
34 D. J. Kedziora and C. Simenel, Phys. Rev. C, **81**: 044613 (2010)
35 K. Sekizawa and K. Yabana, Phys. Rev. C, **93**: 054616 (2016)
36 K. Sekizawa, Phys. Rev. C, **96**: 014615 (2017)
37 Y. Iwata, T. Otsuka, J. A. Maruhn, and N. Itagaki, Phys. Rev. Lett., **104**: 252501 (2010)
38 K. Zhao, Z. Li, Y. Zhang, N. Wang, Q. Li, C. Shen, Y. Wang, and X. Wu, Phys. Rev. C, **94**: 024601 (2016)
39 N. Wang and L. Guo, Phys. Lett. B, **760**: 236 (2016)
40 C. Li, F. Zhang, J. Li, L. Zhu, J. Tian, N. Wang, and F. S. Zhang, Phys. Rev. C, **93**: 014618 (2016)
41 R. Yanez and W. Loveland, Phys. Rev. C, **91**: 044608 (2015)
42 C. Golabek and C. Simenel, Phys. Rev. Lett., **103**: 042701 (2009)
43 N. Vonta et al, Phys. Rev. C, **94**: 064611 (2016)
44 H. M. Devaraja et al, Phys. Lett. B, **748**: 199 (2015)
45 L. Zhu, et al, Phys. Rev. C, **90**: 014612 (2014)
46 L. Zhu, et al, Chin. Phys. C, **40**: 124105 (2016)
47 X. J. Bao, Y. Gao, J. Q. Li, and H. F. Zhang, Phys. Rev. C, **91**: 064612 (2015)
48 X. J. Bao, Y. Gao, J. Q. Li, and H. F. Zhang, Phys. Rev. C, **92**: 034612 (2015)
49 N. Wang, E. G. Zhao, W. Scheid, and S. G. Zhou, Phys. Rev. C, **85**: 041601(R) (2012)
50 Z. Q. Feng, G. M. Jin, J. Q. Li, and W. Scheid, Phys. Rev. C, **76**: 044606 (2007)
51 J. Hong, G. G. Adamian, and N. V. Antonenko, Phys. Lett. B, **764**: 42–48 (2017)
52 W. Nörenberg, Z. Phys. A, **274**: 241–250 (1975)
53 S. Ayik, B. Schürmann, and W. Nörenberg, Z. Phys. A, **277**: 299–310 (1976)
54 P. Möller, J.R. Nix, W. D. Myers, and W. J. Swiatecki, At. Data Nucl. Data Tables, **59**: 185 (1995)
55 L. Zhu et al, Phys. Rev. C, **93**: 064610 (2016)
56 X. J. Bao, S. Q. Guo, H. F. Zhang, and J. Q. Li, J. Phys. G: Nucl. Part. Phys., **43**: 125105 (2016)
57 C. Y. Wong, Phys. Rev. Lett., **31**: 766 (1973)
58 J. Q. Li and G. Wolschin, Phys. Rev. C, **27**: 590 (1983)
59 A. S. Zubov, G. G. Adamian, N. V. Antonenko, S. P. Ivanova, and W. Scheid, Phys. Rev. C, **68**: 014616 (2003)
60 J. D. Jackson, Can. J. Phys, 34: (1956) 767
61 V. F. Weisskopf, Phys. Rev., **52**: 295 (1937)
62 V. F. Weisskopf and D. H. Ewing, Phys. Rev., **57**: 472 (1940)
63 N. Bohr and J. A. Wheeler, Phys. Rev., **56**: 426 (1939)
64 S. Cohen and W.J. Swiatecki, Ann. Phys., **22**: 406 (1963)
65 H. A. Bethe, Phys. Rev., **50**: 332 (1936)
66 W. Loveland, Phys. Rev. C, **76**: 014612 (2007)